nature communications

Article

https://doi.org/10.1038/s41467-024-53448-2

Ionisation of atoms determined by kappa refinement against 3D electron diffraction data

Received: 2 April 2024

Accepted: 8 October 2024

Published online: 21 October 2024

Check for updates

Ashwin Suresh[1,2], Emre Yörük[1], Małgorzata K. Cabaj[1,3], Petr Brázda[1], Karel Výborný[1], Ondřej Sedláček[1], Christian Müller[1,4], Hrushikesh Chintakindi[1,2], Václav Eigner[1] & Lukáš Palatinus[1]

Conventional refinement strategies used for three-dimensional electron diffraction (3D ED) data disregard the bonding effects between the atoms in a molecule by assuming a pure spherical model called the Independent Atom model (IAM) and may lead to an inaccurate or biased structure. Here we show that it is possible to perform a refinement going beyond the IAM with electron diffraction data. We perform kappa refinement which models charge transfers between atoms while assuming a spherical model. We demonstrate the procedure by analysing five inorganic samples; quartz, natrolite, borane, lutecium aluminium garnet, and caesium lead bromide. Implementation of kappa refinement improved the structure model obtained over conventional IAM refinements and provided information on the ionisation of atoms. The results were validated against periodic DFT calculations. The work presents an extension of the conventional refinement of 3D ED data for a more accurate structure model which enables charge density information to be extracted.

3D ED has garnered quite a bit of interest in the past decade with the advent of ultrafast data acquisition techniques, and its capabilities to reveal crystal structures ranging from small unit cells to highly complex systems. Different variants of the method have been continuously researched and developed, such as automated diffraction tomography (ADT), precession electron diffraction tomography (PEDT), continuous rotation electron diffraction (cRED), electron diffraction tomography (EDT), and microcrystal electron diffraction (MicroED)[1–8]. The 3D ED methods benefit from the strong interaction between matter and electrons, making it a more suitable data acquisition technique than single crystal x-ray diffraction, when dealing with very small crystals[1,5,9,10].

Several software packages have been developed or adapted for data reduction, processing, and refinement of the data collected from 3D ED[11–20]. The conventional structure refinement strategies often employ the kinematical approximation, presuming the electrons to be scattered at most once in the crystal and the diffracted intensity to be proportional to the structure-factor amplitude. However, this is a relatively poor approximation as it disregards the multiple scattering of electrons[21–23], which leads to worse figures of merit (R-factors). To correctly describe this phenomenon, the dynamical refinement strategy has been developed[24,25]. This refinement strategy uses the dynamical diffraction theory and Bloch-wave formalism to calculate the diffracted intensities. In the dynamical diffraction theory, the diffracted intensities depend on the crystal thickness (and thus the crystal shape), its orientation relative to the incident beam, and the crystal structure. With dynamical refinement, the fit to the data is greatly improved compared to kinematical refinement, leading to a higher accuracy in the structure parameters[25,26].

Most structure models employed in crystal structure analysis assume the crystal to be a collection of non-interacting isolated atoms with spherical distribution of electron density. This approximation is called the Independent Atom Model (IAM)[27–29]. This model allows the localisation of atoms in the structure, but it does not provide

[1]Institute of Physics of the Czech Academy of Sciences, Prague, Czech Republic. [2]Faculty of Mathematics and Physics, Charles University, Prague, Czech Republic. [3]Biological and Chemical Research Centre, University of Warsaw, Warsaw, Poland. [4]I. Institute for Theoretical Physics, Universität Hamburg, Hamburg, Germany. e-mail: palat@fzu.cz

information on interatomic interactions and the refined atomic displacement parameters and other structure parameters may be inaccurate due to the unfitted bonding effects. A more sophisticated model is needed for two purposes: first, to provide a better insight into the interatomic interactions, and second, to avoid the bias introduced by the IAM into the structure model.

The most commonly used aspherical atom model is the multipole model proposed by Hansen and Coppens and then developed by Stewart, and others[30,31]. The multipole formalism takes into consideration the core electrons, and the spherical and aspherical deformations of the valence electrons to model the electron density as stated in Eq. 1.

$$\rho_{atom}(r) = P_{core}\,\rho_{core}(r) + P_{val}\,\kappa^3\,\rho_{val}(\kappa r) + \sum_{l=0}^{l_{max}} \kappa'^3\,R_l(\kappa' r) \sum_{m=-l}^{l} P_{lm}\,Y_{lm}(\theta,\phi) \quad (1)$$

The first two terms in the equation express the spherical part of the electron density, with P_{core} and P_{val} denoting the population of the core and valence electrons, respectively. The parameter κ scales the radial coordinate r, inducing the expansion or contraction of the spherical part of the valence shell. The third term represents the aspherical part of the valence electron density. R_l describes the radial-type dependency of the aspherical electron density represented by a Slater-type function, and Y_{lm} represents density-normalised real spherical harmonics, with l corresponding to its order and m an integer with $-l \le m \le +l$[28]. Analogous to the parameter κ, the parameter κ' represents the expansion and contraction of the aspherical part. P_{lm} represents the population of electrons in the region described by the real spherical harmonics, thus introducing the asphericity. Y_{lm} integrates to zero over the whole range of θ and ϕ. Thus, the total population of valence electrons depend only on P_{val}.

The charge of an atom q within the multipole formalism can then be calculated as:

$$q = N_{val} - P_{val} \quad (2)$$

where N_{val} represents the number of valence electrons in the neutral state.

The multipole model is commonly used in two ways in structure analysis: (1) multipolar parameters are obtained by fitting them to electron densities calculated by DFT on the investigated structure or a chemically similar fragment, and then kept fixed during the structure refinement[20,32–40], or (2) the multipolar parameters are freely refined against experimental data. The first approach has been proven to improve the fit to experimental data, the accuracy of refined parameters, and particularly, the X-H bond lengths, but because the multipole parameters are not fitted to the data, it does not provide independent information on the charge density distribution, and it is still mostly restricted to organic molecules. In the second approach, the charge density parameters are refined along with the structure parameters against experimental structure factors. This approach has been used to study the bonding effects in both organic and inorganic crystals collected by X-ray diffraction in the past[41–43], but it has not yet been applied to 3D ED data, because these data have been generally regarded as having insufficient quality and accuracy for such a detailed analysis. The charge density studies performed with electron diffraction data mostly involved relatively simple, beam-stable materials and were mostly performed by convergent beam electron diffraction method[44–47]. Due to the intrinsic limitations of this technique, it cannot be generalised to complete 3D studies of more complex materials.

Here, we present the first step towards charge density studies on 3D ED data. We apply a method called kappa refinement which considers only the spherical part of the multipole model, thus retaining the spherical symmetry of the atoms, but allowing adjustment of the valence electron populations and their expansion/contraction as represented by Eq. 3[48].

$$\rho_{atom}(r) = P_{core}\,\rho_{core}(r) + P_{val}\,\kappa^3\,\rho_{val}(\kappa r) \quad (3)$$

The kappa refinement model is thus a simple yet effective extension of the IAM model (introducing only two additional parameters per atom in the refinement) that allows the extraction of the information on charge transfer between the atoms. We demonstrate the general applicability of the method by applying it to a wide range of inorganic structures that vary in the type of chemical bonding, centrosymmetry, crystal morphology, and the atomic number of the constituting atoms. To assess the results, the obtained charge density parameters are compared with refinements performed against theoretical structure factors obtained by DFT calculations.

Results

Performing kappa refinement requires high-quality experimental data. Careful considerations were made to select well-crystallised materials with a low density of imperfections. We chose the following inorganic compounds for the current study:

- α-quartz: chemical formula: SiO_2; $Z = 3$; space group: $P3_221$; unit cell dimensions: $a = 4.9012$ Å, $b = 4.9012$ Å, $c = 5.4068$ Å, $\alpha = 90°$, $\beta = 90°$, $\gamma = 120°$; volume of unit cell: 112.48 Å^3; referred to as *quartz* hereafter.
- natrolite: chemical formula: $Na_2Al_2Si_3O_{12}H_4$; $Z = 8$; space group: *Fdd2*; unit cell dimensions: $a = 18.3885$ Å, $b = 18.7183$ Å, $c = 6.6569$ Å, $\alpha = 90°$, $\beta = 90°$, $\gamma = 90°$; volume of unit cell: 2291.31 Å^3; referred to as *natrolite* hereafter.
- anti-octadecaborane: chemical formula: $B_{18}H_{22}$; $Z = 4$; space group: *Pccn*; unit cell dimensions: $a = 10.7707$ Å, $b = 11.9899$ Å, $c = 10.7360$ Å, $\alpha = 90°$, $\beta = 90°$, $\gamma = 90°$; volume of unit cell: 1386.87 Å^3; referred to as *borane* hereafter.
- caesium lead bromide: chemical formula: $CsPbBr_3$; $Z = 4$; space group: *Pbnm*; unit cell dimensions: $a = 8.1189$ Å, $b = 8.359$ Å, $c = 11.7593$ Å, $\alpha = 90°$, $\beta = 90°$, $\gamma = 90°$; volume of unit cell: 798.1 Å^3; referred to as *Cs-perovskite* hereafter.
- lutetium aluminium garnet: chemical formula: $Lu_3Al_5O_{12}$; $Z = 8$; space group: *Ia-3d*; unit cell dimensions: $a = 11.9105$ Å, $b = 11.9105$ Å, $c = 11.9105$ Å, $\alpha = 90°$, $\beta = 90°$, $\gamma = 90°$; volume of the unit cell: 1689.6 Å^3; referred to as *LuAG* hereafter.

Supplementary Table 1 contains detailed crystallographic information and experimental details, and Supplementary Fig. 1 shows the projections of the structures studied. We focus our study on inorganic compounds for two reasons. First, inorganic compounds are, in general, less prone to radiation damage, making them more suitable for testing the method, and second, inorganic materials, especially heavy-atom compounds, are the most challenging subjects for charge density studies, and their analysis thus puts the method to the ultimate test. Borane is one exception which suffers from radiation damage to some extent but was included in this study in order to test the method on a molecular compound as well. Results on each compound are discussed in detail in the following subsections. 3D ED data were collected using precession and continuous rotation modes for natrolite, precession mode for quartz and borane, and continuous rotation mode for LuAG, and Cs-perovskite. The data were processed using the software PETS2[16]. The beam damage level was evaluated by observing subtle changes in lattice parameters as a function of the total dose[49]. Except for quartz, to prevent beam damage, data for all the other samples were collected at low temperatures (Supplementary Table 1), and the fluence rate was adjusted to prevent beam damage while still recording meaningful intensities at high resolution. The resulting datasets

yielded the correct unit cells with no trends in frame-by-frame magnification corrections, indicating no or negligible radiation damage.

Performing pure kinematical refinements yielded figures of merit (wRall) in the range of 15–25% (Supplementary Table 1) and led to a biased starting model with less accurate structure parameters to perform charge density refinements. Thus accounting for dynamical effects in structural refinements is paramount in obtaining accurate structure models and performing kappa refinements. Both the IAM refinements and the kappa refinements were performed in JANA2020[18] using the dynamical refinement approach. Accurately calculating intensities for dynamical refinements from irregularly shaped crystals with varying thicknesses is difficult[24]. To this end, two models were introduced to approximate the effect of irregular crystal shapes: (1) a model for approximating the shape as a wedge or cylinder[24] and (2) for correction of thickness as a function of the tilting of the crystal. The corrections are explained in detail in the Materials and Methods section. The parameters of the models used for the different compounds in the study and the residual factors (R-factors) before and after the introduction of the thickness models are included in Supplementary Table 2.

The quality of the kappa refinements was evaluated by analysing the difference Fourier maps, static deformation density maps, and the R-factors, and by comparing the experimental results with the results of the refinements against theoretical structure factors obtained from DFT calculations. The static deformation density maps were calculated by subtracting the neutral IAM electron density from the atomic electron density of the kappa model, excluding the smearing effect of the atomic displacement parameters. These maps show the deformation of the valence electron density and depict the level of charge transfer between the atoms. The DFT calculations were performed using two different ab initio methods (implemented in WIEN2k and Crystal23 packages), and theoretical x-ray structure factors corresponding to the optimised electron densities were obtained from these programmes. The Mott-Bethe formula was then used to calculate the electron structure factors from the x-ray structure factors. Kappa refinements on these structure factors were performed to obtain "theoretical" P_{val} and κ values for comparison with the experimentally determined ones. For a more objective comparison between the datasets, we calculated merged R-factors (MR-factors) by performing symmetry-averaging of experimental and calculated intensities after the dynamical refinement[26]. The results of the qualitative and quantitative assessment of the kappa refinements for each of the compounds are presented in the following sub-sections.

IAM refinement of quartz

The data was collected from a lab-grown highly crystalline quartz nanorod[50] essentially devoid of defects using the precession-assisted 3D ED method and had a resolution $(\sin\theta/\lambda)_{max}$ of 1.25 Å^{-1}. The quality of the crystal, the simplicity of the crystal structure, and the atomic number of less than 20 for both the atoms (Z(Si) = 14 and Z(O) = 6) made it a good reference material to check the feasibility of performing the charge density studies on 3D ED data. The dynamical refinements were performed at the resolution of 1.25 Å^{-1}. Quartz has two enantiomorphic forms belonging to the $P3_221$ and $P3_121$ space groups. To determine the absolute structure, the R-factors between the two possible enantiomorphs were compared (Supplementary Table 3). There was a sharp drop in the R-factors when the space group was changed from $P3_121$ (MwRall = 6.98%) to $P3_221$ (MwRall = 3.63%). For the subsequent refinements, this absolute structure was used, and further improvements (MwRall = 3.30%) were obtained by using the cylindric thickness model and the tilt correction parameter of 0.25.

Kappa refinement of quartz and comparison with theoretical calculations

During the kappa refinement, the P_{val} and κ of both Si and O atoms were refined freely along with other structure parameters. The improvement in the difference Fourier maps before and after the kappa refinements is shown in Fig. 1A, B. The improvement in the fit of the structure model after the kappa refinement is evident from the reduced noise level in the difference Fourier map in Fig. 1B and the drop in R-factors from MwRall 3.30% to 2.38%. The results of the experimental refinements were compared with the refinements against structure factors obtained from DFT calculations using the Crystal23 and the WIEN2k programme packages. The P_{val} and κ values of Si and O atoms obtained after the refinements in all three cases were in good agreement (within two e.s.d) with each other, as shown in Table 1. The differences between charge density parameters from refinements on experimental data and the two refinements on theoretical data were smaller than the differences between the two theoretical data sets. The static deformation maps (Fig. 1C–E) show expected features with positive density peaks around the O atom and negative density peaks around the Si atom. This exhibits the accumulation and depletion of charges around the O and Si atoms, respectively, indicating the charge transfer from the Si atom to the O atom.

IAM refinement of natrolite

Natrolite is a hydrated zeolite with a noncentrosymmetric structure. The data was collected using both the precession-assisted 3D ED and continuous rotation 3D ED on the same crystal to $(\sin\theta/\lambda)_{max}$ of 1.1 Å^{-1} and 1 Å^{-1}, respectively. Similar to quartz, the absolute structure was identified by comparing the R-factors of two possible enantiomorphs during the dynamical refinements (Supplementary Table 4). The dynamical refinements were performed at a resolution $(\sin\theta/\lambda)_{max}$ of 1 Å^{-1}. The 2 hydrogen atoms were identified from the difference Fourier maps (Supplementary Fig. 2). The hydrogen atoms were then restrained to have the same ADPs and fixed bond lengths and angles with the oxygen atom (labelled O3). The subsequent refinements were performed with the wedge thickness model and the tilt correction parameter of 0.4. Harmonic displacement parameters were refined for all the atoms. The atom Si1 had non-positive definite ADPs after the refinement against the precession data.

Kappa refinement of natrolite and comparison with theoretical calculations

The P_{val} and κ parameters of the same atomic species in similar chemical environments were restrained from being equal to reduce the risk of overfitting and to get a chemically reasonable model. To stabilise the initial refinements, only P_{val} were refined while the κ parameters were fixed to 1. In the subsequent refinements, both P_{val} and κ parameters were refined simultaneously. The distance and angle restraints applied to the H atoms could also be removed. The R-factors after kappa refinements compared to the IAM refinements are listed in Table 2. The atomic displacement parameters also improved after the kappa refinements for both data sets. The improvement was also evident in the difference Fourier maps (Fig. 2A–D), with a notable reduction of the noise level in the maps after the kappa refinement. The charge density parameters of all the atoms were in good agreement for both the data sets except for the κ values of H atoms (Table 2). The results from the experimental data were then compared with the refinements on structure factors obtained from WIEN2k and Crystal23. The refinement results from the two packages showed similar behaviour, with the P_{val} of the Na atom approaching 0 and the κ value of the Na atom being above 2. This was in contrast to the values obtained from the refinement of the experimental data with the P_{val} of the Na atom around 0.25 and the κ value around 1.3 (Table 2). These subtle differences were also visible in the static deformation maps (Fig. 2E–H). The differences in the maps are primarily due to the variations in the κ values between the data sets. The negative electron density is more concentrated in the Na atoms for the two theoretical data sets because of larger ionisation and larger κ values in comparison

https://doi.org/10.1038/s41467-024-53448-2

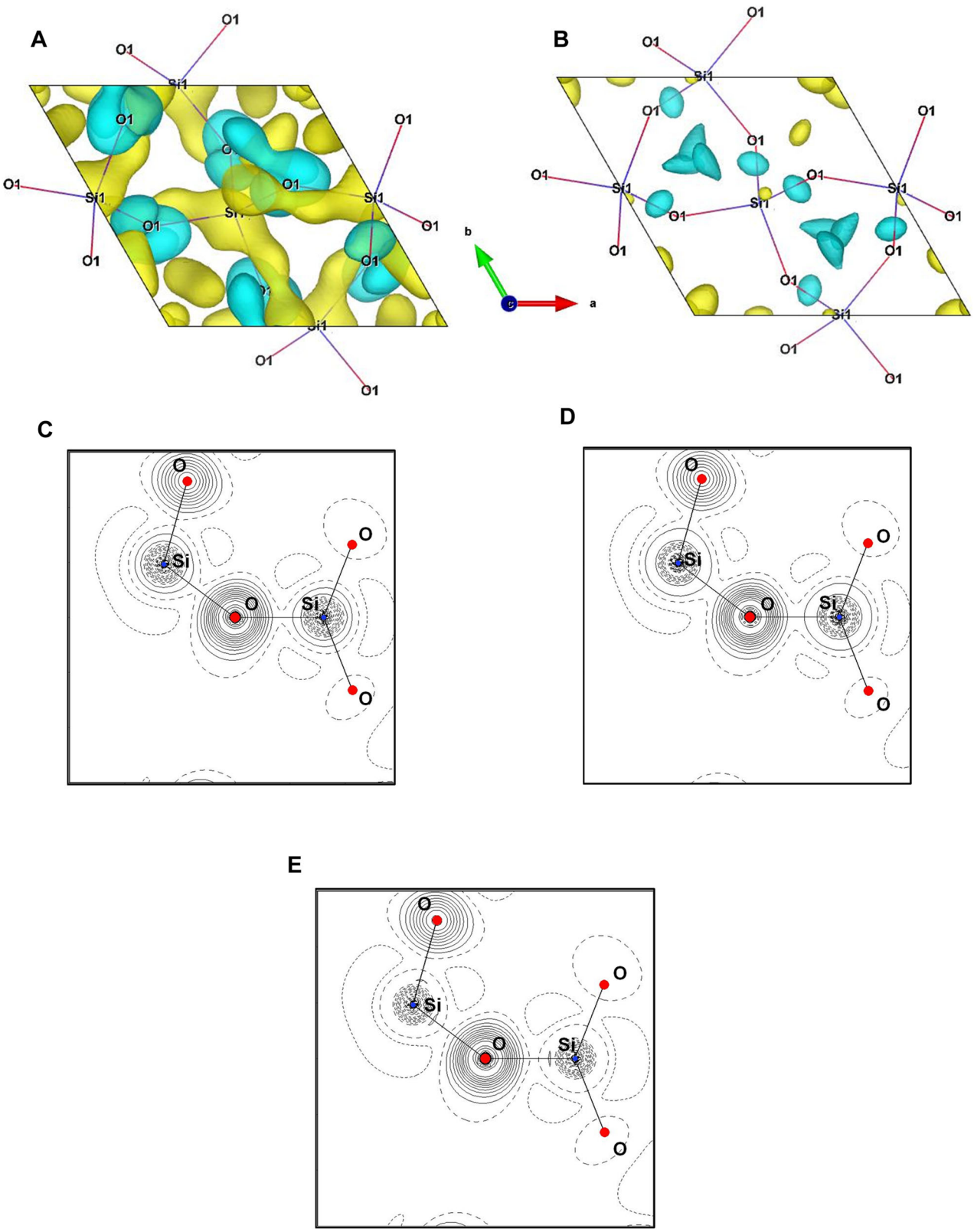

Fig. 1 | Evaluation of quality of refinements for quartz. 3D difference Fourier map of the whole cell after showing improvements in the structure model from the IAM refinement (**A**), and after kappa refinement (**B**) plotted at the same isosurface value (0.07 e Å^{-1}). Positive and negative isosurfaces are plotted in yellow and blue, respectively. The static deformation maps centred around the O atom obtained after the refinement of experimental structure factors (**C**), and theoretical structure factors from WIEN2k (**D**) and Crystal23 (**E**) scaled to the same contour level of 0.045 e Å^{-3}, depicting the accumulation and depletion of charges on O atom and from Si atom respectively. The positive and negative electron density is contoured with full lines and dashed lines, respectively.

Table 1 | Refinement statistics and refined charge density parameters against experimental and theoretical data for Quartz

Sample		Experiment	Theory	
Quartz (SiO_2)				
Method/Programme	–	Precession	WIEN2k	Crystal23
Resolution sinθ/λ ($Å^{-1}$)	–	1.25	1.0	1.25
IAM refinement				
RSg(max), DSg(max)	–	0.70, 0.00	–	–
No. of reflections (Nobs/Nall)	–	5364/7491	600/629	1175/1218
No. of reflections after symmetry averaging (MNobs/MNall)	–	960/1074	600/629	1175/1218
No. of parameters	–	126	1	1
Robs/MRobs	–	3.73/2.52	1.89/1.89	1.27/1.27
Rall/MRall	–	4.61/2.74	1.90/1.90	1.29/1.29
wRall/MwRall	–	4.54/3.30	3.42/3.42	3.02/3.02
GoFobs/GoFall	–	1.38/1.22	2.02/1.98	3.40/3.34
Kappa Refinement				
RSg(max), DSg(max)	–	0.70, 0.00	–	–
No. of reflections (Nobs/Nall)	–	5364/7491	600/629	1175/1218
No. of reflections after symmetry averaging (MNobs/MNall)	–	960/1074	600/629	1175/1218
No. of parameters	–	130	5	5
Robs/MRobs	–	3.18/2.06	0.96/0.96	0.57/0.57
Rall/MRall	–	4.07/2.29	0.97/0.97	0.59/0.59
wRall/MwRall	–	3.64/2.38	1.68/1.68	0.89/0.89
GoFobs/GoFall	–	1.09/0.97	1.00/0.98	1.00/0.99
Number of electrons in the structural unit	–	30	30	30
The sum of valence electrons fixed in the refinement	–	16	16	16
Charge density parameters				
Atom label				
Si1 (N_{val} = 4)	P_{val}	2.870 (45)	2.952 (60)	2.781 (26)
	κ	1.084 (6)	1.097 (7)	1.073 (3)
	q = N_{val} - P_{val}	1.130 (45)	1.048 (60)	1.219 (26)
O1 (N_{val} = 6)	Pval	6.565 (23)	6.524 (30)	6.609 (13)
	κ	0.996 (2)	0.999 (4)	0.994 (1)
	q = N_{val} - P_{val}	− 0.565 (23)	− 0.524 (30)	− 0.609 (13)

to the results from the experimental data sets. The differences in the charge density parameters between the data can be attributed to the difficulty of modelling the diffused 3 s electron in the valence shell of the Na atom. As expected, the maps show negative electron density around the cations and positive electron density around the anions, corresponding to the depletion and accumulation of electrons around cations and anions, respectively.

IAM refinement of borane

Borane is a molecular crystal having two B_9H_{11} subunits connected by a B-B edge. Each subunit forms a cage-like structure[51,52]. Borane has the lightest constituent atoms (with Z(B) = 5 and Z(H) = 1) among the compounds studied. The data was collected using the continuous rotation 3D ED method. The sample diffracted to a resolution $(\sin\theta/\lambda)_{max}$ = 0.85 $Å^{-1}$. The 11 hydrogen atoms in each of the cages were identified from the difference Fourier maps (Supplementary Fig. 3). The dynamical refinements were performed at a resolution $(\sin\theta/\lambda)_{max}$ of 0.85 $Å^{-1}$. The ADPs of all the atoms were refined anisotropically. The subsequent refinements were performed with the wedge thickness model and a tilt correction parameter of 0.25. Two hydrogen atoms (H1b3, and H1b8) had non-positive definite ADPs after the refinement. The MwRall reached 7.11%.

Kappa refinement of borane and comparison with theoretical calculations

Similar to the refinements of natrolite, the P_{val} and κ parameters of the same atomic species in similar chemical environments were restrained from being equal in the kappa refinements. The P_{val} of both B and H atoms refined close to their neutral values except for three H atoms (bridging hydrogens) that are bonded to two B atoms each. The quality of the structure model improved considerably after the refinement, documented by the improvement in R-factors (MwRall = 5.21%, Table 3) and by the notable improvement of the atomic displacement parameters of all the atoms (Fig. 3A, B). The difference Fourier maps in Fig. 3C, D also show a dramatic improvement after the kappa refinement. In comparison to other compounds in this study, borane has a larger ratio of the number of valence electrons to the total number of electrons in its structural unit. Moreover, the electron density in borane behaves in a quasi-aromatic manner[53,54]. Thus, the contribution of the redistribution of valence electrons to the structural model is larger in borane in comparison to others and describing it more accurately improves the structure model considerably. The refinement results were then compared with the refinement results from the structure factors obtained from the Crystal23 work package (Table 3). The P_{val} and κ values of the atoms for the two datasets were in good agreement with each other. In both the experimental and theoretical results, the three bridging hydrogens were more positive than the other atoms, as expected[55–57]. The behaviour is in agreement with the literature[58,59]. Most of the improvement from the IAM refinement to kappa refinement is related to the changes in the expansion/contraction parameter κ and not to the redistribution of electrons between atoms, as the P_{val} refined very close to the neutral values for most of the atoms. The κ parameter for all the atoms of both data sets was more than 1, compensating for the diffused distribution of the valence electrons in borane. The static deformation maps (Fig. 3E, F) also showed similar features with negative density inside the two cages of the molecule. This shows the displacement of electrons from inside the cage to the nearby B and H atoms creating a region of negative difference electron density inside the cage.

IAM refinement of Cs-perovskite

$CsPbBr_3$ has a perovskite structure with tilted $PbBr_6$ octahedra surrounding the Cs atom occupying the high-coordination perovskite-A site[60]. This structure is composed of heavy atoms (Z; Cs = 55, Pb = 82, Br = 35), making it an ideal test material to assess the possibility of obtaining experimental charge density information on heavy atoms. A MwR(all) of 4.90% was obtained from the dynamical refinement using the IAM model, with all atoms refined with anisotropic displacement parameters and using the wedge thickness model. The resolution was set to $(\sin\theta/\lambda)_{max}$ = 1.0 $Å^{-1}$. Refinements using the tilt correction parameter did not yield a notable improvement in the R-factors, suggesting that the apparent thickness did not change greatly during the tilting. Refinements were therefore performed with the tilt correction parameter of 0.

Kappa refinement of Cs-perovskite and comparison with theoretical calculations

Initial kappa refinements showed chemically reasonable charge density parameters except for the Cs site, whose κ could not be refined. This was due to the P_{val} being refined very close to zero,

https://doi.org/10.1038/s41467-024-53448-2

Table 2 | Refinement statistics and refined charge density parameters against experimental and theoretical data for natrolite

Sample		Experiment		Theory	
Natrolite [$Na_2Al_2Si_3O_{12}H_4$]					
Method/Programme	–	Precession	Continuous Rotation	WIEN2k	Crystal23
Resolution sinθ/λ (Å^{-1})	–	1.0	1.0	1.0	1.0
IAM Refinement					
RSg(max), DSg(max)	–	0.66, 0.00	0.66, 0.0015		
No. of reflections (Nobs/Nall)	–	10475/25820	10849/11952	4747/4799	4748/4776
No. of reflections after symmetry averaging (MNobs/MNall)	–	3224/4565	4395/4516	4747/4799	4748/4776
No. of parameters	–	219	157	1	1
Robs/MRobs	–	6.48/5.12	5.67/4.51	1.99/1.99	1.99/1.99
Rall/MRall	–	10.19/6.27	5.85/4.56	1.99/1.99	1.99/1.99
wRall/MwRall	–	7.61/5.75	6.87/5.42	4.32/4.32	4.48/4.48
GoFobs/GoFall	–	1.71/1.19	2.68/2.56	4.21/4.19	6.71/6.70
Kappa Refinement					
RSg(max), DSg(max)	–	0.66, 0.00	0.66, 0.0015		
No. of reflections (Nobs/Nall)	–	10475/25820	10849/11952	4747/4799	4748/4776
No. of reflections after symmetry averaging (MNobs/MNall)	–	3224/4565	4395/4516	4747/4799	4748/4776
No. of parameters	–	235	173	17	17
Robs/MRobs	–	5.68/4.27	4.91/3.74	0.55/0.55	0.43/0.43
Rall/MRall	–	9.48/5.41	5.11/3.80	0.55/0.55	0.43/0.43
wRall/MwRall	–	6.42/4.41	5.83/4.48	1.03/1.03	0.67/0.67
GoFobs/GoFall	–	1.38/1.00	2.27/2.17	1.00/1.00	1.00/1.00
Number of electrons in the structural unit	–	190	190	190	190
The sum of valence electrons fixed in the refinement	–	96	96	96	96
Charge density parameters					
Atom label	–	–	–	–	–
Si1, Si2[a] (N_{val} = 4)	P_{val}	2.836 (50)	2.824 (68)	2.813 (14)	2.781 (10)
	κ	1.068 (8)	1.061 (11)	1.067 (2)	1.029 (2)
	q = N_{val} - P_{val}	1.164 (50)	1.176 (68)	1.187 (14)	1.219 (10)
Al1 (N_{val} = 3)	P_{val}	1.986 (62)	1.769 (82)	1.836 (18)	1.742 (12)
	κ	1.062 (14)	1.064 (22)	1.084 (5)	1.074 (4)
	q = N_{val} - P_{val}	1.014 (62)	1.231 (82)	1.164 (18)	1.258 (12)
Na1 (N_{val} = 1)	P_{val}	0.261 (53)	0.254 (68)	0.021 (9)	0.020 (6)
	κ	1.398 (183)	1.269 (220)	2.307 (903)	2.204 (578)
	q = N_{val} - P_{val}	0.739 (53)	0.746 (68)	0.979 (9)	0.98 (6)
O1 (N_{val} = 6)	P_{val}	6.735 (31)	6.660 (41)	6.663 (9)	6.681 (6)
	κ	0.951 (5)	0.977 (6)	0.968(1)	0.979 (1)
	q = N_{val} - P_{val}	−0.735 (31)	−0.660 (41)	−0.663 (9)	−0.681 (6)
O2 (N_{val} = 6)	P_{val}	6.714 (28)	6.877 (34)	6.791 (8)	6.824 (5)
	κ	0.959 (5)	0.949 (5)	0.955 (1)	0.964 (1)
	q = N_{val} - P_{val}	−0.714 (28)	−0.877 (34)	−0.791 (8)	−0.824 (5)
O3 (N_{val} = 6)	P_{val}	6.713 (44)	6.717 (54)	6.986 (13)	6.994 (9)
	κ	1.040 (7)	1.029 (8)	0.941 (2)	0.948 (1)
	q = N_{val} - P_{val}	−0.713 (41)	−0.717 (54)	−0.986 (13)	−0.994 (9)
O5, O4, O6[a] (N_{val} = 6)	P_{val}	6.749 (28)	6.786 (34)	6.827 (7)	6.859 (5)
	κ	0.964 (4)	0.962 (4)	0.953 (1)	0.962 (1)
	q = N_{val} - P_{val}	−0.749 (26)	−0.786 (34)	−0.827 (7)	−0.859 (5)
H2, H1[a,b] (N_{val} = 1)	P_{val}	0.544 (25)	0.564 (26)	0.501 (5)	0.494 (4)
	κ	1.167 (82)	1.817 (166)	1.605 (23)	1.549 (15)
	q = N_{val} - P_{val}	0.456 (26)	0.436 (26)	0.499 (5)	0.506 (4)

[a]The Pval and κ parameters of atoms in similar chemical environments were constrained to be equal.
[b]The ADPs were constrained to be equal.

leading to an almost singularity in the refinement of κ, as the contraction of an empty valence shell is undefined. Refinements constraining the κ of Cs to different values between 1 and 1.6 showed no notable changes to the rest of the refined parameters. The κ of Cs was then constrained to 1.2, which corresponds to a reasonable expected valence-shell contraction of highly ionised atoms. All other parameters were freely refined. The final charge density parameters are given in Table 4. The refined parameters show substantial ionisation. The Cs atom, which is in the 12-fold coordinated perovskite position, shows an ionisation of about + 0.8. This is supported by the fact that the electronegativity difference between Cs and Br is very large, 2.17 on the Pauling scale. The two Br sites were refined

https://doi.org/10.1038/s41467-024-53448-2

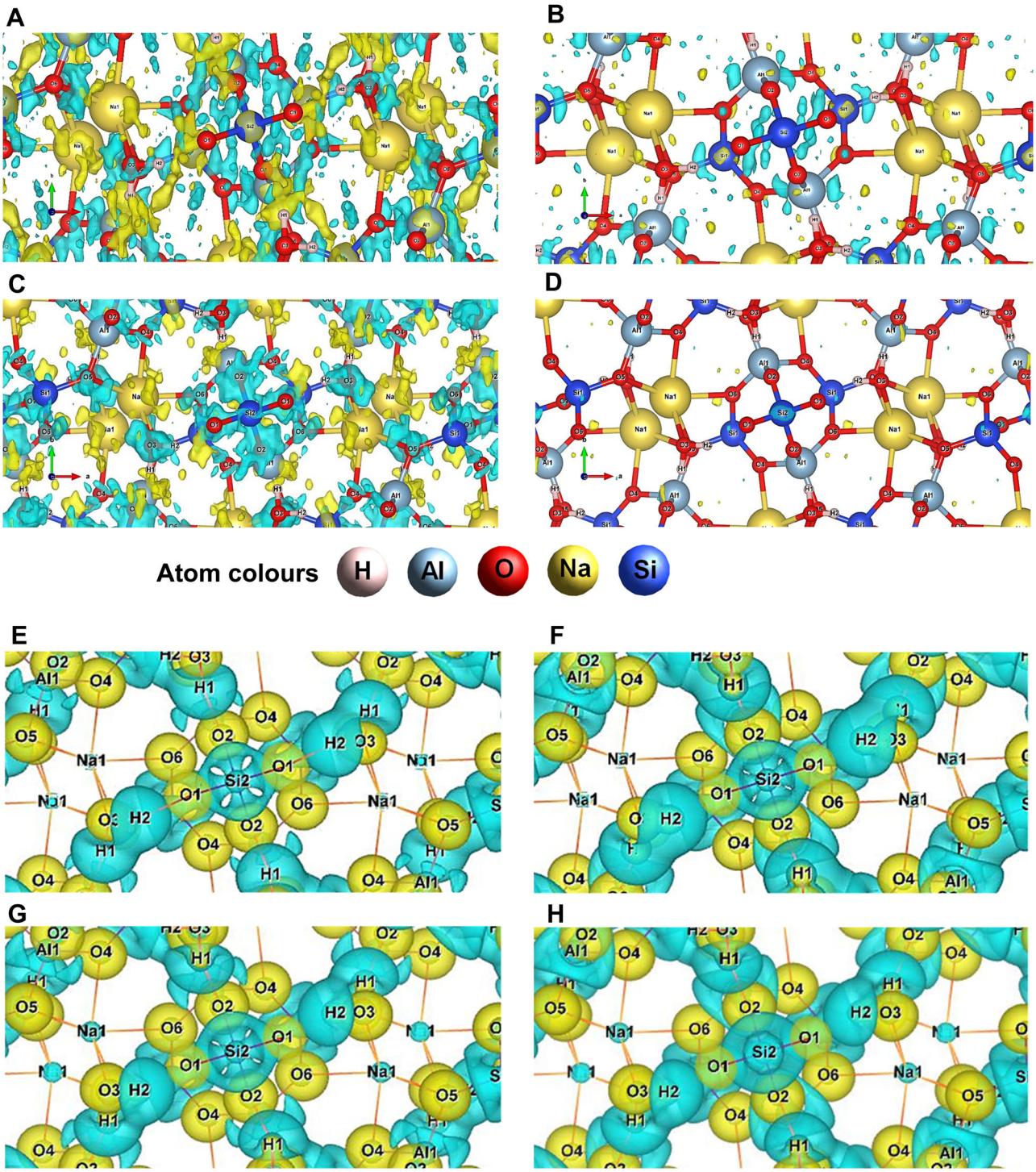

Fig. 2 | Evaluation of quality of refinements for natrolite. 3D difference Fourier map of a section centred around the Si atom after IAM refinement (**A**), and after kappa refinement (**B**) for precession data and after IAM refinement (**C**), and after kappa refinement (**D**) for continuous rotation data plotted at the same isosurface value (0.18 e Å^{-1}). Static deformation maps centred around the Si atom after the refinement of experimental structure factors for precession data (**E**) and continuous rotation data (**F**), and theoretical structure factors from WIEN2k (**G**) and Crystal23 (**H**) and plotted at the same isosurface value (0.1 e Å^{-3} for positive density and 0.04 e Å^{-3} for negative density). Positive and negative isosurfaces are plotted in yellow and blue, respectively.

independently, but similar charge density parameters were obtained. Compared to the IAM refinement, there was an improvement of 0.1% in the R-factors (Table 4). Unlike the compounds described previously, the improvement in the structure model, atomic displacement parameters, and difference Fourier map (Fig. 4A, B) after the refinement was small. This is expected, as the proportion of valence electrons to the total number of electrons in the structural unit for heavy atom compounds is considerably smaller compared to quartz, natrolite or borane. The distribution of charges in the kappa model is visualised in the static deformation maps (Fig. 4C, D). As expected, the maps show electron density accumulation around the anions and depletion around the cations. The maps and ionisation parameters obtained from the refinements on theoretical structure factors obtained from the WIEN2k programme package show good

https://doi.org/10.1038/s41467-024-53448-2

Table 3 | Refinement statistics and refined charge density parameters against experimental and theoretical data for borane

Sample		Experiment	Theory
Borane ($B_{18}H_{22}$)			
Method/Programme		Continuous Rotation	Crystal23
Resolution sinθ/λ (Å^{-1})		0.85	1.25
IAM Refinement			
RSg(max), DSg(max)		0.66, 0.00	
No. of reflections (Nobs/Nall)		4779 /13809	3873/4775
No. of reflections after symmetry averaging (MNobs/MNall)		1906 /3179	3873/4775
No. of parameters		233	1
Robs/MRobs		7.56/6.51	6.63/6.63
Rall/MRall		12.99/8.46	6.69/6.69
wRall/MwRall		8.45/7.11	8.66/8.66
GoFobs/GoFall		2.27/1.44	4.30/3.88
Kappa Refinement			
RSg(max), DSg(max)		0.66, 0.00	
No. of reflections (Nobs/Nall)		4779 /13809	3873/4775
No. of reflections after symmetry averaging (MNobs/MNall)		1906/3179	3873/4775
No. of parameters		249	17
Robs/MRobs		6.04/4.89	1.78/1.78
Rall/MRall		11.44/6.82	1.86/1.86
wRall/MwRall		7.08/5.21	2.23/2.23
GoFobs/GoFall		1.85/1.20	1.10/1.00
Number of electrons in the structural unit		56	56
The sum of valence electrons fixed in the refinement		38	38
Charge density parameters			
Atom labels			
B3 (N_{val} =3)	P_{val}	3.231 (44)	3.119 (11)
	κ	1.054 (9)	1.117 (3)
	$q = N_{val} - P_{val}$	− 0.231 (44)	− 0.119 (11)
B5, B4, B6, B2[a] (N_{val} =3)	P_{val}	3.153 (16)	3.002 (5)
	κ	1.063 (6)	1.145 (2)
	$q = N_{val} - P_{val}$	− 0.153 (16)	− 0.002 (5)
B8, B7, B1[a] (N_{val} =3)	P_{val}	3.06 (19)	3.065 (7)
	κ	1.081 (6)	1.116 (2)
	$q = N_{val} - P_{val}$	− 0.06 (19)	− 0.065 (7)
B9 (N_{val} =3)	P_{val}	3.037 (25)	3.039 (7)
	κ	1.067 (9)	1.116 (3)
	$q = N_{val} - P_{val}$	− 0.037 (25)	− 0.039 (7)
H1b3 (N_{val} =1)	P_{val}	0.957 (24)	0.970 (6)
	κ	1.249 (45)	1.317 (12)
	$q = N_{val} - P_{val}$	0.043 (24)	0.030 (6)
H1b3b7, H1b1b9, H1b3b8[a] (N_{val} =1)	P_{val}	0.772 (14)	0.847 (4)
	κ	1.46 (4)	1.323 (8)
	$q = N_{val} - P_{val}$	0.228 (14)	0.153 (4)
H1b5, H1b4, H1b6, H1b2[a] (N_{val} =1)	P_{val}	0.923 (10)	1.023 (3)
	κ	1.394 (23)	1.272 (5)
	$q = N_{val} - P_{val}$	0.077 (10)	− 0.023 (3)
H1b7, H1b8, H1b1[a] (N_{val} =1)	P_{val}	0.992 (8)	1.012 (3)
	κ	1.28 (2)	1.268 (5)
	$q = N_{val} - P_{val}$	0.008 (8)	− 0.012 (3)

[a]The Pval and κ parameters of atoms in similar chemical environments were constrained to be equal.

agreement with those obtained from the experiments (Fig. 4E, F) (Table 4). It was possible to refine the κ value of Cs (κ = 1.65) from the theoretical data, which indicates a very strong contraction as expected. Experimental data also show a strong Pb ionisation, despite a smaller electronegativity difference with Br (1.09). The theoretical data, however, show a weaker ionisation with a smaller contraction. Further tests showed that refining the experimental data with κ of Pb being constrained to the value obtained from the theoretical data, a weaker Pb ionisation is refined (+ 0.64), which matches its theoretical counterpart. In contrast to κ of Cs, the κ of Pb had a notable impact on the refined parameters. This is attributed to the lower ionisation of Pb in comparison to Cs and the effect of κ to accurately define the remaining population of electrons in Pb. The ionisation of Br sites is slightly stronger in the experimental data compared to the theoretical data. Despite the notable differences between the experimental and theoretical charge density parameters, this result shows that it is possible to extract information about atomic ionisation from experimental data that is at least in a semiquantitative agreement with the DFT calculations. It should also be noted that the parameters obtained by DFT cannot be taken as a ground truth without reservation.

IAM refinement of LuAG

In LuAG the Lu atom is coordinated to 8 O atoms, and the Al atom is in two distinct octahedral and tetragonal coordination states[61]. The presence of a heavy atom (Z; Lu = 71) and two distinct Al sites represent an ideal case for testing the validity of kappa refinement on inorganic compounds. Initial IAM refinement with a resolution of $(\sin\theta/\lambda)_{max}$ = 1.3 Å^{-1} resulted in an MwR(all) of 5.91%, and switching from isotropic to harmonic displacement parameters had a small impact (MwRall = 5.91% to 5.68%), consistent with an isotropic character of the displacements. The improvement gained from using the wedge thickness model was comparable to $CsPbBr_3$ (MwRall = 5.68% to 4.27%). As with Cs-Perovskite, attempts at thickness correction using the tilt correction parameter did not improve the statistics, so the refinements were carried out with the wedge thickness model and the tilt correction parameter of 0.

Kappa refinement of LuAG and comparison with theoretical calculations

Initial kappa refinements were unstable due to the κ value of Lu being refined to unreasonably large values, with the indication of notable ionisation. Since it was challenging to refine the κ value of Lu in a stable manner, the κ was scanned in the range from 1 to 2 with a step size of 0.05, which covers the range of expected values. At each step, the κ value of Lu was constrained, and all other parameters were refined. The evolution of the weighted R-factors calculated for high- and low-resolution reflections is given in Supplementary Fig. 4. The separation point of $(\sin\theta/\lambda)_{max}$ of 0.22 Å^{-1} was chosen as the estimated limit of charge sensitivity by comparing the electron scattering factors of charged and neutral atoms. It can be seen that the high-resolution reflections are insensitive to the variation, while R-factors of the low-resolution reflections go down steadily until reaching a plateau at the κ value of Lu = 1.75. In this range, the P_{val} of Lu varies from 1.48 to 0.69 as κ increases (Supplementary Fig. 5). Given that the two Al positions show comparable but weaker ionisation compared to Lu, along with κ values close to 1.1, a κ(Lu) value of 1.30 was chosen to correspond to a stronger ionisation and contraction of the electron density, taking into account the larger difference in electronegativity between Lu-O compared to Al-O. The charge density parameters obtained after the refinement with κ(Lu) fixed to 1.3 are given in Table 5. Similarly to the Cs-perovskite, there was only a small improvement in the difference Fourier map (Fig. 5A, B) and the R-factors after the kappa refinement. Lu, which is in an 8-fold coordination state with O with a high electronegativity difference (2.17), shows strong ionisation. The Al sites

https://doi.org/10.1038/s41467-024-53448-2

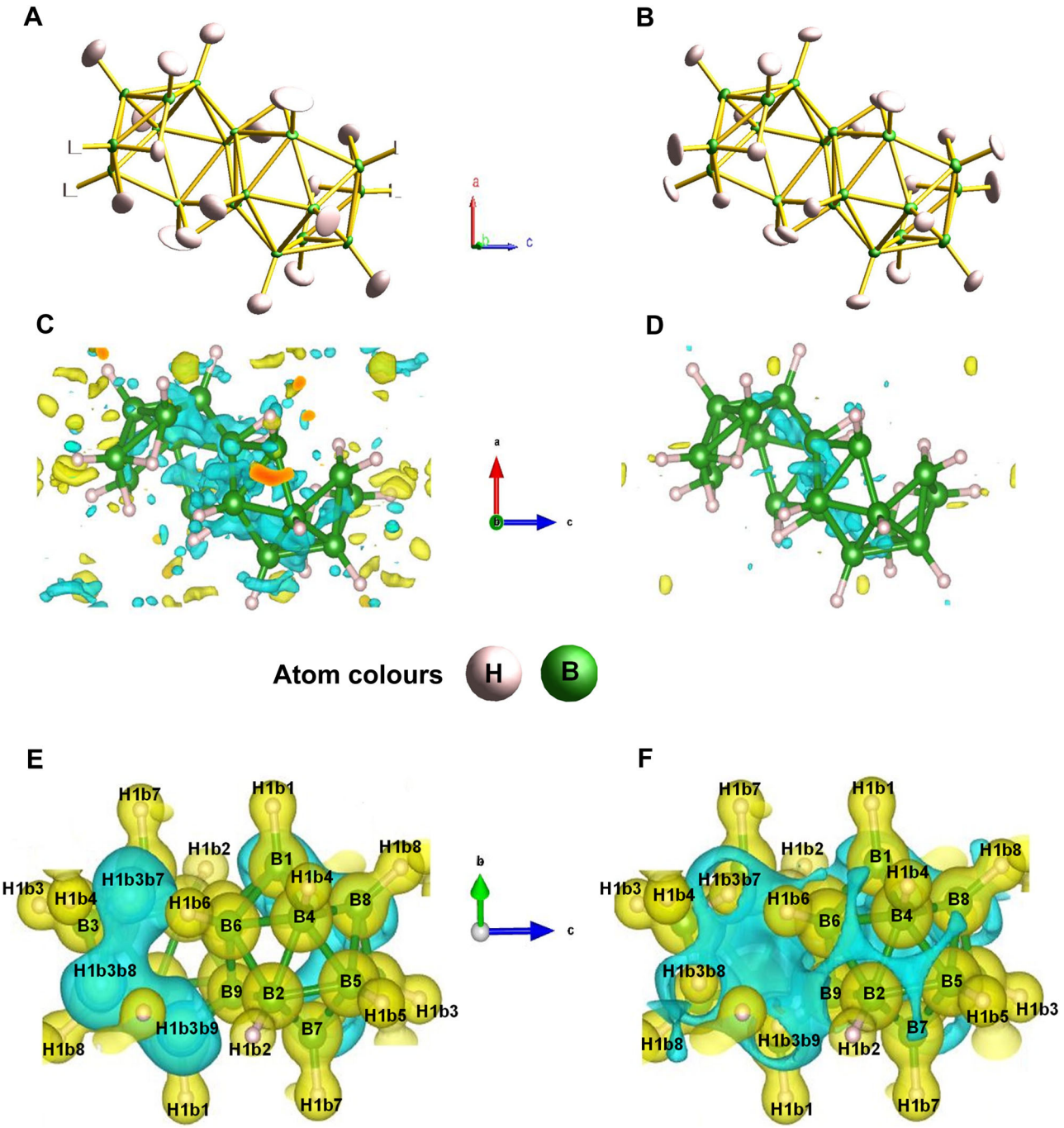

Fig. 3 | Evaluation of quality of refinements for borane. Structure model of the compound after IAM refinement (**A**) where green boxes indicate non-positive definite displacement parameters of the boron atoms, which gets better after the kappa refinement (**B**). The 3D difference Fourier map after IAM refinement (**C**), and after kappa refinement (**D**) is plotted at the same isosurface value (0.15 e Å^{-1}). Static deformation maps of the molecule after the refinement of experimental structure factors (**E**) and theoretical structure factors from Crystal23 (**F**) plotted at the same isosurface value (0.045 e Å^{-3}). Positive and negative isosurfaces are plotted in yellow and blue, respectively.

show a less strong but notable ionisation, per a relatively high Al-O electronegativity difference (1.83). Furthermore, Al2, which is in octahedral coordination, shows a stronger ionisation compared to Al1 in tetrahedral coordination (Fig. 5C, D), which is expected because of the larger distance from the oxygen atoms in the octahedral coordination. Kappa refinement was also performed on theoretical electron structure factors obtained using linearised augmented plane wave method (LAPW) with GGA functional as implemented in the WIEN2k programme package, and the maps and charge parameters obtained are given in Fig. 5E, F and Table 5 respectively. Both the maps and the charge parameters show good agreement with the experiment. It was possible to refine κ(Lu) from the theoretical data to a value of 1.336, which is in good agreement with the value constrained for the experimental data. A comparison of ionisation values shows a good agreement, with the DFT showing slightly less strong ionisation overall. The only noticeable difference is seen for the κ(Al2), which refined to 1.245 compared to 1.030 obtained from the experimental data. Given the strong ionisation observed for Al2 which is in an octahedral coordination, it is possible that the contraction was underestimated for the experimental data.

Table 4 | Refinement statistics and refined charge density parameters against experimental and theoretical data for Cs-perovskite

Sample		Experiment	Theory
Caesium lead bromide ($CsPbBr_3$)			
Method/Programme	–	Continuous Rotation	WIEN2k
Resolution sinθ/λ (Å–1)	–	1.0	1.0
IAM Refinement			
RSg(max), DSg(max)	–	0.66, 0.0015	
No. of reflections (Nobs/Nall)	–	2709/16345	3271/3366
No. of reflections after symmetry averaging (MNobs/MNall)	–	1086/3314	3271/3366
No. of parameters	–	87	1
Robs/MRobs	–	5.48/4.64	0.23/0.23
Rall/MRall	–	16.10/9.00	0.24/0.24
wRall/MwRall	–	6.79/4.90	1.17/1.17
GoFobs/GoFall	–	1.45/0.70	9.59/9.45
Kappa Refinement			
RSg(max), DSg(max)	–	0.66, 0.0015	0.7, 0.0015
No. of reflections (Nobs/Nall)	–	2709/16345	3271/3366
No. of reflections after symmetry averaging (MNobs/MNall)	–	1086/3314	3271/3366
No. of parameters	–	94	9
Robs/MRobs	–	5.40/4.57	0.08/0.08
Rall/MRall	–	16.03/8.92	0.09/0.09
wRall/MwRall	–	6.58/4.61	0.12/0.12
GoFobs/GoFall	–	1.39/0.68	1.01/1.00
Number of electrons in the structural unit	–	242	242
The sum of valence electrons fixed in the refinement	–	26	26
Charge density parameters			
Atom labels			
Cs (N_{val} =1)	P_{val}	0.163 (75)	0.220 (4)
	κ	1.2[a]	1.647(17)
	$q = N_{val} - P_{val}$	0.837 (75)	0.780 (4)
Pb (N_{val} = 4)	P_{val}	2.584 (69)	3.243(4)
	κ	1.290 (28)	1.084 (1)
	$q = N_{val} - P_{val}$	1.416 (69)	0.757 (4)
Br1 (N_{val} = 7)	P_{val}	7.750 (44)	7.512 (3)
	κ	0.941(4)	0.976 (3)
	$q = N_{val} - P_{val}$	−0.750 (44)	−0.512 (3)
Br2 (N_{val} = 7)	P_{val}	7.753 (54)	7.512 (3)
	κ	0.938(6)	0.976 (3)
	$q = N_{val} - P_{val}$	−0.753 (54)	−0.512 (3)

[a]The κ parameter was fixed for the refinement

Discussion

The current work focused on the kappa refinement strategy to model 3D ED data. The refinement strategy improves on the conventional dynamical structure refinements and extracts information about charge transfer between the atoms. We studied the scope of the refinements on five known inorganic materials with different structural motifs collected by 3D ED. Among the studied compounds, borane exhibited the largest improvement of the structure model after the kappa refinement (Table 3 and Fig. 3A, B) because of the strong influence of the valence electrons in the structure model and the quasi-aromatic behaviour of borane. In contrast, for structures with heavy elements, like Cs-perovskite and LuAG, the expected improvement in the figures of merit and the quality of the structure model is minimal because the large shielding effect from the core electrons in these atoms reduces the effect of valence electrons on the total atomic density.

Charge density studies give insight into atomic interactions in organic and inorganic materials. These studies can be extended to a wide variety of applications, studying macromolecular systems, proteins, magnetic molecular compounds, porous materials, etc[1]. Electrons are scattered by both negatively charged electron cloud and positively charged nucleus, whereas X-ray is scattered only by the negatively charged electron cloud[62]. The strong interaction of electrons with matter in comparison to X-rays enables users to analyse very small crystals of the size of a few nanometres[1]. Our results show that the kappa refinement (and, by extension, other models of charge density redistribution) may be an important part of the refinement procedure for structures with light atoms, even in cases where the actual charge density information is not explicitly needed. The results from kappa refinements against X-ray data from natrolite (Supplementary Table 5) and borane (Supplementary Table 6) show difficulties in refining the H atom with improbable values for the kappa parameter. Meanwhile, charge density studies on heavy atoms are rare and difficult, but the higher sensitivity of electrons to the bonding effects than X-rays[63] allows us to study the finer details of the electron densities even in these cases, where X-ray data is extremely difficult or impossible. The usefulness of the kappa model against 3D ED data can also be gauged by the improved atomic displacement parameters and the distances of the hydrogen atoms, as shown in the case of natrolite and borane.

The results of the kappa refinement were validated qualitatively by comparing the refined values to the general trends expected from the basic chemical considerations. Inspection of Tables 1–5 shows that all atoms with expected positive ionisation (cations) exhibited a decrease in the valence shell population, while anions (O, Br) had, without exception, an increase in the valence shell population. Hydrogen atoms were positively ionised when bonded to oxygen, but almost neutral when bonded to boron. Thus, the results of the kappa refinement show a remarkable qualitative agreement with the expected behaviour. Note that this chemical information is not forced on the structure model in any way, and these are genuinely independent experimental observations.

In light of the shortcomings of X-ray diffraction, an objective quantitative evaluation with X-ray data as the reference cannot be made, especially since the charge density parameters of hydrogen atoms were unreliable. Quantitative evaluation was thus performed by comparison of the κ and P_{val} parameters refined against noise-free, simulated data from electron densities calculated by DFT approaches using two different ab initio methods (implemented in Crystal23 and WIEN2k). Interestingly, where both programmes were used, the difference between them was of a similar magnitude to the difference between the experimental and DFT parameters. In general, the agreement between the experimental parameters and the DFT-derived ones was good, with an average absolute error between the experimental charges and the DFT-derived ones for light atoms and heavy atoms (excluding Pb) being less than 0.1 and 0.2 electrons, respectively. The worst disagreement was obtained for the ionisation of Pb, with the difference of 0.66(7) electrons, i.e., 9.4σ. Pb is the heaviest atom in our study, and the disagreement with the DFT may indicate that we hit the limits of the achievable accuracy with the present data. Difficulties were also encountered when modelling the diffuse s electrons in the valence shell of atoms Na, Cs, and Lu. Refining their precise

https://doi.org/10.1038/s41467-024-53448-2

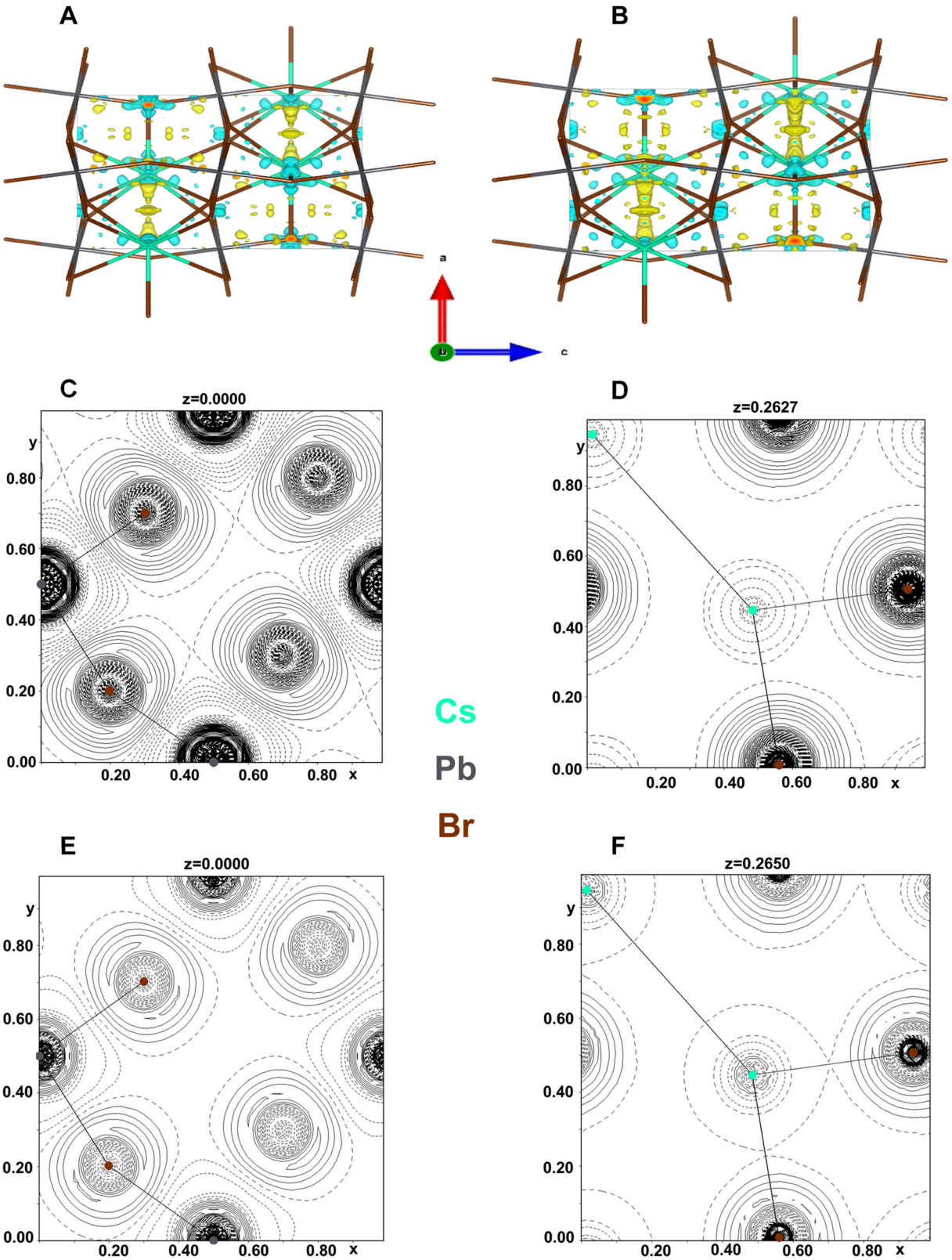

Fig. 4 | Evaluation of quality of refinements for Cs-perovskite. 3D difference Fourier map of the molecule after IAM refinement (**A**), and after kappa refinement (**B**) plotted at the same isosurface value (0.33 e Å^{-1}). The positive and negative isosurfaces are plotted in yellow and blue, respectively. 2D Static deformation maps were obtained after the refinement of experimental structure factors (**C**, **D**), and theoretical structure factors from WIEN2k (**E**, **F**) with the contour level 0.01 e Å^{-3}. The positive and negative electron density is contoured with full lines and dashed lines, respectively. Letters x, y and z denote the fractional coordinates in the sections.

Table 5 | Refinement statistics and refined charge density parameters against experimental and theoretical data for LuAG

Sample		Experiment	Theory
Lutetium Aluminium Garnet ($Lu_3Al_5O_{12}$)			
Method/Programme	–	Continuous Rotation	WIEN2k
Resolution sinθ/λ (Å^{-1})	–	1.3	1.0
IAM Refinement			
RSg(max), DSg(max)	–	0.66, 0.0015	
No. of reflections (Nobs/Nall)	–	7493/21544	434/599
No. of reflections after symmetry averaging (MNobs/MNall)	–	1016/1302	434/599
No. of parameters	–	66	1
Robs/MRobs	–	7.25/4.42	1.05/1.05
Rall/MRall	–	11.94/5.16	1.13/1.13
wRall/MwRall	–	8.20/4.87	3.90/3.90
GoFobs/GoFall	–	1.73/1.14	1.30/1.18
Kappa Refinement			
RSg(max), DSg(max)	–	0.66, 0.0015	0.7, 0.0015
No. of reflections (Nobs/Nall)	–	7493/21544	434/599
No. of reflections after symmetry averaging (MNobs/MNall)	–	1016/1302	434/599
No. of parameters	–	73	9
Robs/MRobs	–	7.15/4.27	0.72/0.73
Rall/MRall	–	11.77/5.01	0.73/0.73
wRall/MwRall	–	8.09/4.73	3.30/3.30
GoFobs/GoFall	–	1.70/1.12	1.18/1.00
Number of electrons in the structural unit	–	374	374
The sum of valence electrons fixed in the refinement	–	96	96
Charge density parameters			
Atom labels			
Lu (N_{val} = 3)	P_{val}	1.136 (73)	1.302 (291)
	κ	1.3[a]	1.336(291)
	q = N_{val} - P_{val}	1.864 (73)	1.698 (291)
Al1 (N_{val} = 3)	P_{val}	1.660 (108)	1.732 (227)
	κ	1.103 (34)	1.131 (70)
	q = N_{val} - P_{val}	1.340 (108)	1.268 (227)
Al2 (N_{val} = 3)	P_{val}	1.224 (288)	1.340 (344)
	κ	1.030 (93)	1.245 (146)
	q = N_{val} - P_{val}	1.776 (288)	1.660 (344)
O (N_{val} = 6)	P_{val}	7.097 (80)	7.018 (165)
	κ	0.903(8)	0.933 (17)
	q = N_{val} - P_{val}	−1.097 (80)	−1.018 (165)

[a]The κ parameter was fixed for the refinement

population and contraction parameters is difficult, as their contribution to the scattering factors lies in a few lower-order reflections[43,64–68]. This observation is not unique to the present work; examples in the literature show that the κ of these atoms often needs to be constrained to unity[69–72].

The kappa refinement and other refinement strategies for extracting charge density information do not explicitly define the chemical charge of an atom. They give an insight into the redistribution of the population of electrons within the atomic electron density and provide an estimation of the atomic ionisation. The other limitation and an important requirement to perform these refinements is the need for good quality data from good quality crystals with very few crystal imperfections (single-phase, single-domain non-deformed crystal with low mosaicity), high completeness (more than 85%), and good resolution ($(\sin\theta/\lambda)_{max}$ of 0.75 Å^{-1}).

Although kappa refinement does not take into consideration the aspherical part of the Hassens-Coppens multipolar model, the capability to extract reasonable charge density parameters and improve the fit of the structure model while still assuming a simple spherical approximation is beneficial for more accurate structure refinements.

The current work is the backbone of our ongoing efforts to develop workflows for accurate structure refinements and charge density analysis from 3D ED data.

Methods

Sample preparation

Quartz and borane samples were provided by the authors of ref. 50 and ref. 54 respectively, in which the syntheses are mentioned. The natrolite sample was of natural origin, found at Marianska Skala, Usti nad Labem, Czech Republic. The quartz sample was transferred to the Cu holey grid by gently pressing the grid against the nanocrystalline powder, and the borane and natrolite samples were crushed in a mortar before transferring to the TEM grid. The sample of Cs-perovskite was synthesised as described in ref. 73. It was available as a suspension in toluene with a concentration of 0.8 mg/ml. The mother solution was diluted 20 times to achieve a reasonable concentration of crystals for TEM analysis. The diluted solution was ultrasonicated for 15 mins. A drop was then introduced onto a Cu holey carbon TEM grid, and the toluene was removed by evaporation. LuAG samples were obtained as a pellet with the synthesis technique described in ref. 74. The pellet was cut with scissors and crushed very gently to obtain a nanocrystalline powder, which was then spread over a Cu holey carbon TEM grid.

Data collection & processing

All electron diffraction measurements were performed on an FEI Tecnai G2 20 (LaB6 filament, 200 kV) microscope equipped with a hybrid pixel detector (Medipix 3 ASI Cheetah). Samples were deposited on Cu holey-carbon TEM grids. These were mounted on a single tilt holder and inserted into the TEM sample stage. 3D ED data for quartz was collected using the hybrid pixel detector in precession mode, with the help of the Nanomegas DigiSTAR precession unit. Data on samples borane, LuAG, and Cs-perovskite were collected using the hybrid pixel detector in continuous rotation mode. Two datasets from the natrolite sample were collected by hybrid pixel detector in precession and continuous rotation modes from the same crystal. The microscope and the detector were piloted by in-house scripts within the software iTEM. Crystal tracking during the tilting of the goniometer was performed using the Fast-ADT routine[11]. Parameters relevant to the data collection are given in Supplementary Table 1. Except for quartz, the data were collected at low temperatures to reduce thermal displacements, which could potentially correlate with the distribution of the electron density. Adjustment of the beam intensity also played a crucial role in the data quality. The irradiation has to be sufficiently strong to record the weaker high-resolution reflections reliably, but a too-strong irradiation leads to some strong low-resolution reflection intensities saturating the dynamic range of the detectors. Depending on how strongly each crystal diffracted, an intermediate level of irradiation was chosen, and saturated reflections detected by PETS2 were discarded.

Data acquisition was optimised to obtain datasets suitable for the refinement of the charges. The crystal quality of individual particles

https://doi.org/10.1038/s41467-024-53448-2

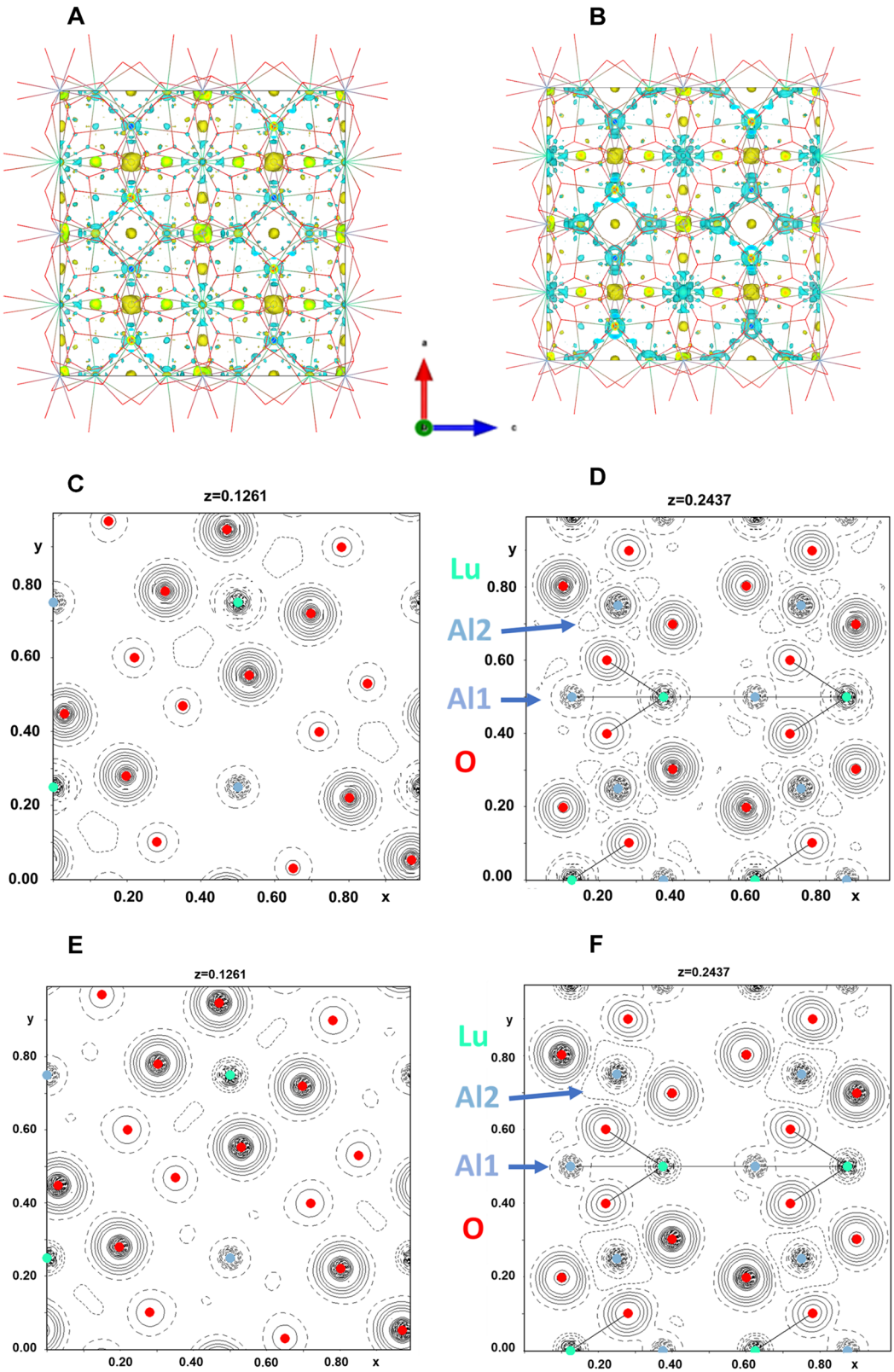

Fig. 5 | Evaluation of quality of refinements for LuAG. 3D difference Fourier map of the molecule after IAM refinement (**A**), and after kappa refinement (**B**) plotted at the same isosurface value (0.50 e Å^{-1}). The positive and negative isosurfaces are plotted in yellow and blue, respectively. 2D Static deformation maps were obtained after the refinement of experimental structure factors (**C**, **D**), and theoretical structure factors from WIEN2k (**E**, **F**) with the contour level 0.05 e Å^{-3}. The positive and negative electron density is contoured with full and dashed lines, respectively. Letters x, y and z denote the fractional coordinates in the sections.

was assessed by observing their diffraction contrast in TEM image mode. Diffracting particles with well-defined morphology (Supplementary Fig. 1) were checked under the TEM alpha-wobbler to see whether the diffraction contrast evolves in a uniform manner, which is an indicator of a single-phase, single-domain non-deformed crystal.

PETS2 software was used for data reduction and processing. Data from every crystal was processed separately. This included creating a list of peak coordinates by peak-searching on raw diffraction images, which is then used in the determination of the orientation matrix and the lattice parameters of the unit cell. The optical distortions were then refined[49], and the frame orientations were optimised[75]. For kinematical refinements, integrated intensities were obtained, and symmetry-equivalent reflections were averaged. For dynamical refinement from precession 3D ED data, the intensities were integrated frame-by-frame[18], while for the continuous rotation data, the data for the refinement were generated using the concept of overlapping virtual frames[26].

IAM refinement

All structures presented in this study were solved and refined using the JANA2020 software[18]. For structure solutions, the charge-flipping algorithm implemented in Superflip[17] was used for all the compounds. The validity of the structure solutions was confirmed by comparing them to the previously solved structures. The structures were then initially refined within the kinematical approximation. This was then followed by dynamic refinements. These were performed using the in-house developed Dyngo software integrated into JANA2020. For each dataset, one scale factor per frame and one thickness parameter (t_o) per dataset were refined in an initial refinement cycle with all other parameters fixed, before letting all parameters refine in parallel. In further refinement cycles, anisotropic displacement parameters and thickness models were gradually introduced to increase the accuracy of the models. The quality of the refinements was assessed by analysing the R-factors and the amplitude of features in the difference electrostatic potential maps.

Handling of crystal thickness in dynamical refinement

Exact calculations for the diffracted intensities of a crystal with an irregular shape are difficult. However, assuming the validity of the column approximation, the need for the exact description of the crystal shape can be reduced to the need to know the probability distribution function of thickness across the crystal[24]. A wedge, a cylinder, or a lens are examples of some basic geometric shapes that can be used to approximate the shape of the crystal and further simplify the problem. For these shapes, the cumulative distribution function corresponding to the thickness probability distribution function can be obtained analytically[24]. A command *thick model* followed by the name of the geometric shape can be passed to Dyngo commands in the '*Edit parameters for electron diffraction*' form in JANA2020, and the calculations of dynamical diffraction intensities in Dyngo then perform the calculations taking the selected model of the crystal shape into account.

The second important problem is the issue of the changes in the thickness with the crystal tilt. When the crystal is tilted in 3D ED, the thickness along the incoming beam changes as a function of the tilt angle. For an ideal, infinitely large plate with constant thickness and oriented perpendicular to the beam at zero tilt, the thickness for a given tilt angle θ is given by "$t(\theta) = t_o/cos\theta$", where t_o is the thickness at $\theta = 0°$. This is one extreme case. The other extreme case occurs when the crystal is isometric, and its thickness distribution measured along the beam does not change with the tilt. In this case, "$t(\theta) = t_o$". The real situation is likely to be somewhere in between these two extreme cases. An empirical correction can thus be introduced by mixing the two extreme cases. Using an adjustable "tilt correction parameter" C ($0 \le C \le 1$). The thickness as a function of the tilt angle θ is calculated as

$$t(\theta) = C\frac{t_0}{\cos\theta} + (1 - C)t_0 \quad (4)$$

To use this model, the 'Apply correction for crystal tilt' option in the 'Edit parameters for electron diffraction' form of JANA2020 needs to be checked, and the command thickcorr followed by a value between 0 and 1 is written in the text box 'Dyngo commands'. For example, the entire command defining the crystal shape model cylinder and tilt correction parameter of 0.25 that was used for the refinements of quartz was thick model *cylinder thickcorr 0.25*.

It is very difficult to determine the real thickness of crystals from TEM imaging. We estimated the crystal dimensions (Supplementary Table 1) by studying the crystal images obtained at different tilt angles during the data collection. It was difficult to estimate the thickness of the borane crystal because it was not possible to calculate from the crystal projections due to the size of the crystal and the presence of other crystals nearby. The thickness obtained after the refinements is the best available representation of the actual thickness of the crystal.

Kappa refinement

JANA2020 was used to perform the kappa refinements The Mott-Bethe formula was used to convert the X-ray structure factors to electron structure factors. The refinements used form factors from STO wave functions implemented in JANA2020. For the kappa refinements, the structures obtained from the IAM refinements were used as starting models. As with the IAM refinements, the intensities were calculated according to the theory of dynamical diffraction, and the refinements were performed using the same settings as the IAM refinements. The initial values of P_{val} were taken as the number of valence electrons in the neutral state, and all κ values were initially set to unity.

Charge densities calculated with the kappa model were visualised using static deformation maps. These maps are obtained by subtracting the IAM model charge density from the one obtained from the kappa model without the atomic displacement parameters, allowing us to visualise the accumulation or depletion of the electron density.

DFT calculations and refinements

Periodic DFT calculations were performed on the structures of the studied compounds by considering different functionals and wavefunctions (Supplementary Tables 7–11). DFT calculations for quartz, natrolite, and borane were performed using Crystal23 software[76], and the wavefunction was obtained with B3LYP[77,78] functional and pob-TZVP[79] basis set. For quartz, natrolite, Cs-perovskite and LuAG, the electron density and corresponding structure factors were also calculated using WIEN2k software[80] using linearised augmented plane wave method (LAPW) with GGA functional. No optimisation of lattice parameters or atomic positions was performed.

X-ray structure factors obtained from the theoretical electron densities were converted into electron structure factors using the Mott-Bethe formula[81]. The electron scattering factors were then imported into JANA2020, and kinematical refinements were performed against these data using both IAM and the kappa formalism. In these refinements, all displacement parameters were constrained to 0, and the coordinates of the atoms were constrained to the values used in the DFT calculation. Thus, only the scale factors and the charge density parameters were refined.

Data availability

All data needed to evaluate the conclusions in the paper are present in the paper and/or the Supplementary Materials. The data reduction and processing files (PETS2 files), the dynamical refinement files (JANA2020 files), the refinement files for theoretical structure factors

(JANA2020 files), and the CIF files of all the compounds used in the study are available at https://doi.org/10.5281/zenodo.13359514 a repository hosted by Zenodo. Source data are provided in this paper.

References

1. Gemmi, M. et al. 3D Electron diffraction: The nanocrystallography revolution. *ACS Cent. Sci.* **5**, 1315–1329 (2019).
2. Kolb, U., Gorelik, T. & Otten, M. T. Towards automated diffraction tomography. Part II—Cell parameter determination. *Ultramicroscopy* **108**, 763–772 (2008).
3. Gemmi, M. & Oleynikov, P. Scanning reciprocal space for solving unknown structures: energy filtered diffraction tomography and rotation diffraction tomography methods. *Z. Kristallogr. Cryst. Mater.* **228**, 51–58 (2013).
4. Boullay, P., Palatinus, L. & Barrier, N. Precession electron diffraction tomography for solving complex modulated structures: the case of Bi5Nb3O15. *Inorg. Chem.* **52**, 6127–6135 (2013).
5. Jones, C. G. et al. The cryoEM method microED as a powerful tool for small molecule structure determination. *ACS Cent. Sci.* **4**, 1587–1592 (2018).
6. Zhang, D., Oleynikov, P., Hovmöller, S. & Zou, X. Collecting 3D electron diffraction data by the rotation method. *Z. F.ür. Krist.* **225**, 94–102 (2010).
7. Yuan, S. et al. Ti8Zr2O12(COO)16] Cluster: An ideal inorganic building unit for photoactive metal-organic frameworks. *ACS Cent. Sci.* **4**, 105–111 (2018).
8. Cichocka, M. O., Ångström, J., Wang, B., Zou, X. & Smeets, S. High-throughput continuous rotation electron diffraction data acquisition via software automation. *J. Appl. Crystallogr.* **51**, 1652–1661 (2018).
9. Ge, M., Zou, X. & Huang, Z. Three-dimensional electron diffraction for structural analysis of beam-sensitive metal-organic frameworks. *Crystals* **11**, 263 (2021).
10. Yörük, E., Klein, H. & Kodjikian, S. Dose symmetric electron diffraction tomography (DS-EDT): Implementation of a dose-symmetric tomography scheme in 3D electron diffraction. *Ultramicroscopy* **255**, 113857 (2024).
11. Plana-Ruiz, S. et al. Fast-ADT: A fast and automated electron diffraction tomography setup for structure determination and refinement. *Ultramicroscopy* **211**, 112951 (2020).
12. Sheldrick, G. M. Crystal structure refinement with SHELXL. *Acta Crystallogr. Sect. C Struct. Chem.* **71**, 3–8 (2015).
13. Wan, W., Sun, J., Su, J., Hovmöller, S. & Zou, X. Three-dimensional rotation electron diffraction: software RED for automated data collection and data processing. *J. Appl. Crystallogr.* **46**, 1863–1873 (2013).
14. Clabbers, M. T. B., Gruene, T., Parkhurst, J. M., Abrahams, J. P. & Waterman, D. G. Electron diffraction data processing with DIALS. *Acta Crystallogr. Sect. Struct. Biol.* **74**, 506–518 (2018).
15. Burla, M. C. et al. Crystal structure determination and refinement via SIR2014. *J. Appl. Crystallogr.* **48**, 306–309 (2015).
16. Palatinus, L. et al. Specifics of the data processing of precession electron diffraction tomography data and their implementation in the program PETS2.0. *Acta Crystallogr. Sect. B Struct. Sci. Cryst. Eng. Mater.* **75**, 512–522 (2019).
17. Palatinus, L. & Chapuis, G. SUPERFLIP – a computer program for the solution of crystal structures by charge flipping in arbitrary dimensions. *J. Appl. Crystallogr.* **40**, 786–790 (2007).
18. Petříček, V., Palatinus, L., Plášil, J. & Dušek, M. Jana2020 – a new version of the crystallographic computing system Jana. *Z. F.ür. Krist. Cryst. Mater.* **238**, 271–282 (2023).
19. Dolomanov, O. V., Bourhis, L. J., Gildea, R. J., Howard, Ja. K. & Puschmann, H. OLEX2: a complete structure solution, refinement and analysis program. *J. Appl. Crystallogr.* **42**, 339–341 (2009).
20. Guillot, B., Viry, L., Guillot, R., Lecomte, C. & Jelsch, C. Refinement of proteins at subatomic resolution with MOPRO. *J. Appl. Crystallogr.* **34**, 214–223 (2001).
21. Zou, X. et al. *Electron Crystallography: Electron Microscopy and Electron Diffraction*. (Oxford University Press, Oxford, New York, 2011).
22. *Transmission Electron Microscopy: Diffraction, Imaging, and Spectrometry*. (Springer, Cham, Switzerland, 2016).
23. Hammond, C. *The Basics of Crystallography and Diffraction*. (Oxford University Press: Oxford; New York, 2001.
24. Palatinus, L., Petříček, V. & Corrêa, C. A. Structure refinement using precession electron diffraction tomography and dynamical diffraction: theory and implementation. *Acta Crystallogr. Sect. Found. Adv.* **71**, 235–244 (2015).
25. Palatinus, L. et al. Structure refinement using precession electron diffraction tomography and dynamical diffraction: tests on experimental data. *Acta Crystallogr. Sect. B Struct. Sci. Cryst. Eng. Mater.* **71**, 740–751 (2015).
26. Klar, P. B. et al. Accurate structure models and absolute configuration determination using dynamical effects in continuous-rotation 3D electron diffraction data. *Nat. Chem.* **15**, 848–855 (2023).
27. Genoni, A. et al. Quantum crystallography: Current developments and future perspectives. *Chem. Eur. J.* **24**, 10881–10905 (2018).
28. Guillot, B., Jelsch, C. & Macchi, P. in *10 Multipole Modeling with MoPro and XD* 235–268 (De Gruyter, 2021).
29. Gruza, B., Chodkiewicz, M. L., Krzeszczakowska, J. & Dominiak, P. M. Refinement of organic crystal structures with multipolar electron scattering factors. *Acta Crystallogr. Sect. Found. Adv.* **76**, 92–109 (2020).
30. Hansen, N. K. & Coppens, P. Testing aspherical atom refinements on small-molecule data sets. *Acta Crystallogr. A* **34**, 909–921 (1978).
31. Stewart, R. F. Electron population analysis with rigid pseudoatoms. *Acta Crystallogr. A* **32**, 565–574 (1976).
32. Kulik, M. & Dominiak, P. M. Electron density is not spherical: the many applications of the transferable aspherical atom model. *Comput. Struct. Biotechnol. J.* **20**, 6237–6243 (2022).
33. Jha, K. K. et al. Multipolar atom types from theory and statistical clustering (MATTS) data bank: restructurization and extension of UBDB. *J. Chem. Inf. Model.* **62**, 3752–3765 (2022).
34. Pichon-Pesme, V., Lecomte, C. & Lachekar, H. On building a data bank of transferable experimental electron density parameters applicable to polypeptides. *J. Phys. Chem.* **99**, 6242–6250 (1995).
35. Brock, C. P., Dunitz, J. D. & Hirshfeld, F. L. Transferability of deformation densities among related molecules: atomic multipole parameters from perylene for improved estimation of molecular vibrations in naphthalene and anthracene. *Acta Crystallogr. B* **47**, 789–797 (1991).
36. Nelyubina, Y. V., Korlyukov, A. A., Lyssenko, K. A. & Fedyanin, I. V. Transferable aspherical atom modeling of electron density in highly symmetric crystals: A case study of alkali-metal nitrates. *Inorg. Chem.* **56**, 4688–4696 (2017).
37. Malinska, M. & Dauter, Z. Transferable aspherical atom model refinement of protein and DNA structures against ultrahigh-resolution X-ray data. *Acta Crystallogr. Sect. Struct. Biol.* **72**, 770–779 (2016).
38. Jelsch, C., Pichon-Pesme, V., Lecomte, C. & Aubry, A. Transferability of multipole charge-density parameters: Application to very high resolution oligopeptide and protein structures. *Acta Crystallogr. D. Biol. Crystallogr.* **54**, 1306–1318 (1998).
39. Jelsch, C. et al. Accurate protein crystallography at ultra-high resolution: Valence electron distribution in crambin. *Proc. Natl. Acad. Sci. USA* **97**, 3171–3176 (2000).

40. Olech, B., Brázda, P., Palatinus, L. & Dominiak, P. M. Dynamical refinement with multipolar electron scattering factors. *IUCrJ* **11**, 309–324 (2024).
41. Lippmann, T. et al. Charge-density analysis of YBa2Cu3O6.98. Comparison of theoretical and experimental results. *Acta Crystallogr. A* **59**, 437–451 (2003).
42. Koritsánszky, T. et al. Accurate experimental electronic properties of DL-proline monohydrate obtained within 1 Day. *Science* **279**, 356–358 (1998).
43. Schmøkel, M. S. et al. Atomic properties and chemical bonding in the pyrite and marcasite polymorphs of FeS2: a combined experimental and theoretical electron density study. *Chem. Sci.* **5**, 1408–1421 (2014).
44. Avilov, A., Lepeshov, G., Pietsch, U. & Tsirelson, V. Multipole analysis of the electron density and electrostatic potential in germanium by high-resolution electron diffraction. *J. Phys. Chem. Solids* **62**, 2135–2142 (2001).
45. Wu, J. S. & Spence, J. C. H. Structure and bonding in alpha-copper phthalocyanine by electron diffraction. *Acta Crystallogr. A* **59**, 495–505 (2003).
46. Friis, J., Jiang, B., Spence, J., Marthinsen, K. & Holmestad, R. Extinction-free electron diffraction refinement of bonding in SrTiO3. *Acta Crystallogr. A* **60**, 402–408 (2004).
47. Wu, L., Meng, Q. & Zhu, Y. Mapping valence electron distributions with multipole density formalism using 4D-STEM. *Ultramicroscopy* **219**, 113095 (2020).
48. Coppens, P. et al. Net atomic charges and molecular dipole moments from spherical-atom X-ray refinements, and the relation between atomic charge and shape. *Acta Crystallogr. A* **35**, 63–72 (1979).
49. Brázda, P., Klementová, M., Krysiak, Y. & Palatinus, L. Accurate lattice parameters from 3D electron diffraction data. I. Optical distortions. *IUCrJ* **9**, 735–755 (2022).
50. Pastero, L., Turci, F., Leinardi, R., Pavan, C. & Monopoli, M. Synthesis of α-Quartz with controlled properties for the investigation of the molecular determinants in silica toxicology. *Cryst. Growth Des.* **16**, 2394–2403 (2016).
51. Simpson, P. G. & Lipscomb, W. N. MOLECULAR STRUCTURE OF B18H22. *Proc. Natl. Acad. Sci. USA* **48**, 1490–1491 (1962).
52. Londesborough, M. G. S. et al. Distinct photophysics of the isomers of B18H22 explained. *Inorg. Chem.* **51**, 1471–1479 (2012).
53. King, R. B. Three-dimensional aromaticity in polyhedral boranes and related molecules. *Chem. Rev.* **101**, 1119–1152 (2001).
54. Cerdán, L., Braborec, J., Garcia-Moreno, I., Costela, A. & Londesborough, M. G. S. A borane laser. *Nat. Commun.* **6**, 5958 (2015).
55. Guter, G. A. & Schaeffer, G. W. THE STRONG ACID BEHAVIOR OF DECABORANE. *J. Am. Chem. Soc.* **78**, 3546–3546 (1956).
56. Heřmánek, S. & Plotová, H. Chemistry of boranes. XXII. The acidity of boranes. *Collect. Czechoslov. Chem. Commun.* **36**, 1639–1643 (1971).
57. Hamilton, E. J. M. et al. A stacking interaction between a bridging hydrogen atom and aromatic π density in the n-B18H22–benzene system. *Chem. Eur. J.* **12**, 2571–2578 (2006).
58. Olsen, F. P., Vasavada, R. C. & Hawthorne, M. F. The chemistry of n-B18H22 and i-B18H22. *J. Am. Chem. Soc.* **90**, 3946–3951 (1968).
59. Londesborough, M. G. S. et al. Effect of iodination on the photophysics of the laser borane anti-B18H22: generation of efficient photosensitizers of oxygen. *Inorg. Chem.* **58**, 10248–10259 (2019).
60. Møller, C. K. Crystal structure and photoconductivity of Cæsium plumbohalides. *Nature* **182**, 1436–1436 (1958).
61. Euler, F. & Bruce, J. A. Oxygen coordinates of compounds with garnet structure. *Acta Crystallogr.* **19**, 971–978 (1965).
62. Kulik, M., Chodkiewicz, M. L. & Dominiak, P. M. Theoretical 3D electron diffraction electrostatic potential maps of proteins modeled with a multipolar pseudoatom data bank. *Acta Crystallogr. Sect. Struct. Biol.* **78**, 1010–1020 (2022).
63. Mott., S. N. F. & Massey, S. H. S. W. *The Theory of Atomic Collisions*. (Clarendon Press, 1965).
64. Stevens, E. D., DeLucia, M. L. & Coppens, P. Experimental observation of the effect of crystal field splitting on the electron density distribution of iron pyrite. *Inorg. Chem.* **19**, 813–820 (1980).
65. Coppens, P. X-Ray diffraction and the charge distribution in transition metal complexes. *Coord. Chem. Rev.* **65**, 285–307 (1985).
66. Farrugia, L. J. & Evans, C. Experimental X-ray charge density studies on the binary carbonyls Cr(CO)6, Fe(CO)5, and Ni(CO)4. *J. Phys. Chem. A* **109**, 8834–8848 (2005).
67. Farrugia, L. J., Evans, C., Lentz, D. & Roemer, M. The QTAIM approach to chemical bonding between transition metals and carbocyclic rings: A combined experimental and theoretical study of (η5-C5H5)Mn(CO)3, (η6-C6H6)Cr(CO)3, and (E)-{(η5-C5H4)CF═CF(η5-C5H4)}(η5-C5H5)2Fe2. *J. Am. Chem. Soc.* **131**, 1251–1268 (2009).
68. Stokkebro Schmøkel, M., Overgaard, J. & Brummerstedt Iversen, B. Experimental electron density studies of inorganic materials. *Z. F.ür. Anorg. Allg. Chem.* **639**, 1922–1932 (2013).
69. Zhurov, V. V., Zhurova, E. A. & Pinkerton, A. A. Chemical bonding in cesium uranyl chloride based on the experimental electron density distribution. *Inorg. Chem.* **50**, 6330–6333 (2011).
70. Pant, A. K. & Stevens, E. D. Experimental electron-density-distribution study of potassium iron disulfide, a low-dimensional material. *Phys. Rev. B* **37**, 1109–1120 (1988).
71. Bats, J. W. & Fuess, H. Deformation density in complex anions. III. Potassium perchlorate. *Acta Crystallogr. B* **38**, 2116–2120 (1982).
72. Yeh, S. K., Wu, S. Y., Lee, C. S. & Wang, Y. Electron-density distribution in a crystal of dipotassium tetrafluoronickelate, K2NiF4.
73. Děcká, K. et al. Scintillation response enhancement in nanocrystalline lead halide perovskite thin films on scintillating wafers. *Nanomaterials* **12**, 14 (2022).
74. Jan Pejchal et al. Luminescence and scintillation properties of Mg-codoped LuAG:Pr single crystals annealed in air. *J. Lumin.* **181**, 277–285 (2017).
75. Brázda, P., Palatinus, L. & Babor, M. Electron diffraction determines molecular absolute configuration in a pharmaceutical nanocrystal. *Science* **364**, 667–669 (2019).
76. Erba, A. et al. CRYSTAL23: A Program for computational solid state physics and chemistry. *J. Chem. Theory Comput.* **19**, 6891–6932 (2023).
77. Lee, C., Yang, W. & Parr, R. G. Development of the colle-salvetti correlation-energy formula into a functional of the electron density. *Phys. Rev. B* **37**, 785–789 (1988).
78. Becke, A. D. Density-functional thermochemistry. III. The role of exact exchange. *J. Chem. Phys.* **98**, 5648–5652 (1993).
79. Vilela Oliveira, D., Laun, J., Peintinger, M. F. & Bredow, T. BSSE-correction scheme for consistent gaussian basis sets of double- and triple-zeta valence with polarization quality for solid-state calculations. *J. Comput. Chem.* **40**, 2364–2376 (2019).
80. Blaha, P. et al. WIEN2k: An APW+lo program for calculating the properties of solids. *J. Chem. Phys.* **152**, 074101 (2020).
81. Mott, N. F. & Bragg, W. L. The scattering of electrons by atoms. *Proc. R. Soc. Lond. Ser. Contain. Pap. Math. Phys. Character* **127**, 658–665 (1997).

Acknowledgements

We thank F.Turci (University of Turin) for providing the quartz samples and Michael G. S. Londesborough (Institute of Inorganic Chemistry of the Czech Academy of Sciences) for providing the borane samples. We acknowledge Polish high-performance computing infrastructure PLGrid (HPC Centre: ACK Cyfronet AGH) for providing computer facilities and support within computational grant no. PLG/2023/016082.

Author contributions

Conceptualisation: L.P.; 3D ED Data collection: E.Y., P.B. and H.C.; XRD Data collection: V.E.; Data reduction, processing, and refinements: A.S., E.Y., P.B. and L.P.; Theoretical. calculations: M.K.C., K.V., O.S. and C.M.; Supervision: L.P.; Writing—original draft: A.S. and E.Y.; Writing—review & editing: All authors contributed to the review and editing collaboratively.

Funding

The work is supported by the; H2020 ITN project NanED, grant agreement No. 956099 (L.P., A.S. and H.C.). Czech Science Foundation 3DED-QCr, grant agreement No. 21-44862L (L.P. and E.Y.). OP-JAK project TERAFIT, grant agreement No. CZ.02.01.01/00/22_008/0004594 (K.V.).

Competing interests

The authors declare no competing interests.

Additional information

Supplementary information The online version contains supplementary material available at https://doi.org/10.1038/s41467-024-53448-2.

Correspondence and requests for materials should be addressed to Lukáš. Palatinus.

Peer review information *Nature Communications* thanks the anonymous reviewer(s) for their contribution to the peer review of this work. A peer review file is available.